Korean J Physiol Pharmacol 2024;28(6):503-513
https://doi.org/10.4196/kjpp.2024.28.6.503

KJPP

Original Article

Protective effect of 6′-Sialyllactose on LPS-induced macrophage inflammation *via* regulating Nrf2-mediated oxidative stress and inflammatory signaling pathways

Hami Yu[1,#], Yujin Jin[1,#], Hyesu Jeon[3], Lila Kim[2], and Kyung-Sun Heo[1,*]

[1]*College of Pharmacy and Institute of Drug Research and Development, Chungnam National University, Daejeon 34134,* [2]*GeneChem Inc., Daejeon 34025,* [3]*Department of Cancer AI & Digital Health, National Cancer Center, Goyang 10408, Korea*

ARTICLE INFO

Received March 19, 2024
Revised June 3, 2024
Accepted June 21, 2024

***Correspondence**
Kyung-Sun Heo
E-mail: kheo@cnu.ac.kr

Key Words
Acute inflammation
Oxidative stress
6′-sialyllactose

[#]These authors contributed equally to this work.

ABSTRACT Macrophages play a central role in cardiovascular diseases, like atherosclerosis, by accumulating in vessel walls and inducing sustained local inflammation marked by the release of chemokines, cytokines, and matrix-degrading enzymes. Recent studies indicate that 6'-sialyllactose (6'-SL) may mitigate inflammation by modulating the immune system. Here, we examined the impact of 6'-SL on lipopolysaccharide (LPS)-induced acute inflammation using RAW 264.7 cells and a mouse model. *In vivo*, ICR mice received pretreatment with 100 mg/kg 6'-SL for 2 h, followed by intraperitoneal LPS injection (10 mg/kg) for 6 h. *In vitro*, RAW 264.7 cells were preincubated with 6'-SL before LPS stimulation. Mechanistic insights were gained though Western blotting, qRT-PCR, and immunofluorescence analysis, while reactive oxygen species (ROS) production was assessed *via* DHE assay. 6'-SL effectively attenuated LPS-induced p38 MAPK and Akt phosphorylation, as well as p65 nuclear translocation. Additionally, 6'-SL inhibited LPS-induced expression of tissue damage marker MMP9, IL-1β, and MCP-1 by modulating NF-κB activation. It also reduced ROS levels, mediated by p38 MAPK and Akt pathways. Moreover, 6'-SL restored LPS-suppressed Nrf2 and HO-1 akin to specific inhibitors SB203580 and LY294002. Consistent with *in vitro* results, 6'-SL decreased oxidative stress, MMP9, and MCP-1 expression in mouse endothelium following LPS-induced macrophage activation. In summary, our findings suggest that 6'-SL holds promise in mitigating atherosclerosis by dampening LPS-induced acute macrophage inflammation.

INTRODUCTION

Cardiovascular disease is a leading cause of mortality worldwide [1]. Mainly, cardiovascular disease caused by atherosclerosis, a chonic inflammatory disease of vessel [2]. Numerous studies indicated that toxic agents come from diets, smoke, or oxidized low-density lipoprotein was induced inflammation in various organs [3-5]. Structurally, after various cells are increased levels of pro-inflammatory cytokines or chemokines releasement, its-immune response accelerates immune cell developments [6]. Macrophages are one of the major cell types of the immune systems and regulates inflammation and infection though antigen presentation, polarization, and phagocytosis [1]. Activated macrophages are secreted cytokines or nitric oxides that induces endothelial cell (EC) dysfunction and increased number of abnormal vascular smooth muscle cell [7-9]. In that times, macrophage-derived matrix metalloproteinase-9 (MMP9) expression was involved in macrophage infiltration by destroying collagen in EC [10]. Finally, complex of MMPs and macrophage activation increased development of atherosclerotic plaque formation [10].

Author contributions: H.Y., Y.J., and K.S.H. contributed to study concepts and design. H.Y., Y.J., and H.J. were involved in experimental studies and data acquisition. H.Y., Y.J., H.J., and L.K. conducted data analysis and statistical analysis. H.Y. and Y.J. were wrote manuscript draft and K.S.H. was responsible for finalizing manuscript. All authors read and approved the final manuscript.

Lipopolysaccharides (LPS) has been used for inducing inflammation-mediated damage models in liver, kidney, lung, and EC [4,5,8,11,12]. Mechanistically, LPS lead to activation of inflammatory signaling pathway including mitogen activated protein kinase (MAPK), protein kinase B (Akt), and nuclear factor kappa-light chain enhancer of activated B cells (NF-κB) [8]. p38/MAPK, one of the MAPKs, plays a significant role in inflammation by releasing inflammatory mediators such as tumor necrosis factor-α interleukins (ILs), and monocyte chemoattractant protein-1 (MCP-1) [11]. Activation of p38 also contributes to macrophage polarization and migration though Akt phosphorylation, exacerbating the progression of atherosclerosis [11].

Reactive oxygen species (ROS) can lead to immune dysfunction and impaired cell proliferation when deficient in the cell. However, the excessive release of superoxide radicals, generated by macrophages activated due to cellular oxidative stress, can lead to apoptosis, aging, and inflammatory diseases [7]. Therefore, antioxidants are used to protect cells and tissues from high concentrations of ROS caused by oxidative stress. Nuclear factor erythoid 2-related factor 2 (Nrf2), a transcriptional regulator of intracellular oxidative stress, undergoes increased translocation into the nucleus in response to inflammation-stimulating factors. This translocation leads to the release of antioxidants, which can inhibit ROS and suppress inflammation [13].

Sialyllactose (SL) is the one of the components on human milk oligosaccharides, which is the third major solid component in breast milk, are recognized as the first beneficial nutrient in infants [14]. There are two different structures of SLs that 3'-SL and 6'-SL which is recognized by linking with monosaccharides N-acetylneuraminic acid on and the galactosyl subunit of lactose at the 3' or 6' position, respectively [11]. Our group have been reported that 3'-SL or 6'-SL exert a wide range of pharmacological effects on acute liver injury, EC hyperpermeability, and phenotypic switching of vascular smooth muscle cell [3,4,8,15]. However, the effects of 6'-SL on LPS-induced macrophage activation on atherosclerosis progression and its-related signaling pathway remain unclear. This study aimed to investigate the effect of 6'-SL on LPS-induced macrophage activation in *in vitro* and *in vivo*.

METHODS

Reagents and antibodies

Rabbit antibodies against phosphorylation NF-κB p65 (Ser546) (#3033S), NF-κB (#8242), phosphorylation Akt (Ser473) (#4058), Akt (#2685), phosphorylation p38 (Th180/Th182) (#4631), p38 (#8690), Nrf2 (#12721), poly ADP-ribose polymerase (PARP) (#9532) were purchased from Cell Signaling Technology, Inc. Rabbit antibodies against MCP-1 (sc-28879) and mouse antibodies against β-tubulin (sc-166729) were purchased from Santa Cruz Biotechnology. Rabbit antibody MMP9 (AB19016) was purchased from Merck Milipore. Rat antibody against vascular endothelial-cadherin (VE-cadherin, #555289) was purchased from BD Biosciences. 6'-SL salt powder was purchased from GeneChem Inc. LPS (from *Escherichia coli* O111:B4, EL2630) was purchased from Sigma-Aldrich. SB203580 (S7741), an inhibitor of p38, and LY294002 (S1105), and inhibitor of Akt were purchased from Selleckchem. Phosphate buffered saline (PBS, #EBA-1105) was purchased from Elpisbio.

Cell culture

The murine macrophage cell line, RAW 264.7 (#40071), was procured from the Korean Cell Line Bank. Cells were maintained in Dulbecco's Modified Eagle's Medium (Gibco), supplemented with 10% fetal bovine serum (Gibco) and 1% penicillin/streptomycin (100 U/ml, Gibco), and incubated at 37°C in a 5% CO_2 humidified environment.

Cell viability

RAW 264.7 cells were plated in a 96-well plate and then incubated at 37°C with 5% CO_2 for 24 h. Subsequently, the cells were pre-treated with varying concentrations of 6'-SL for 1 h before being stimulated with 1 μg/ml of LPS for another 24 h. Cell viability was assessed using the 3-(4,5-dimethylthiazole-2-yl)-2,5-diphenyltetrazolium bromide assay (MTT, Sigma-Aldrich), with absorbance readings taken at 570 nm using a microplate reader (SpectraMax iD3; Molecular Devices).

Measurement of ROS level

ROS production was assessed using the dihydroethidium (DHE) assay (#D11347, Invitrogen). RAW 264.7 cells were seeded in 12-well plates and incubated overnight at 37°C with 5% CO_2. Following treatment, the cells were incubated with 10 μM DHE in PBS for 45 min at 37°C. Subsequently, the cells were washed, fixed in 4% formaldehyde for 10 min, and then washed again and kept in 1X PBS. Fluorescence images of DHE-stained cells were captured using a fluorescence microscope (Olympus IX 71; Olympus). The intensity of DHE fluorescence was analyzed using ImageJ software.

Nuclear and cytoplasmic extraction

RAW 264.7 cells were collected using PBS and centrifuged at 13,000 rpm for 1 min at 4°C. Nuclear extraction was conducted following a previously reported method with minor adjustments [16]. Cells were incubated with a hypotonic buffer containing 100 mM 4-(2-hydroxyethyl)-1-piperazineethanesulfonic acid (pH 7.9), 1 M KCl, 100 mM 1,4-Dithiothreitol (DTT), and 1X protease inhibitor cocktails for 5 min. Subsequently, 10% NP-40 was added, and the mixture was incubated on ice for 15 min. The samples

were then centrifuged at 5,000 rpm for 5 min, and the resulting supernatant contained cytoplasmic proteins. The pellet was washed with PBS, resuspended in a hypertonic buffer comprising 100 mM 4-(2-hydroxyethyl)-1-piperazineethanesulfonic acid (pH 7.9), 2.5 M NaCl, 100 mM DTT, and 1X protease inhibitor cocktails, and incubated on ice for 15 min. After centrifugation at 13,000 rpm for 10 min, the supernatant was collected as nuclear protein. Finally, 20 μl of the samples were loaded onto sodium dodecyl sulfate–polyacrylamide gel electrophoresis (SDS-PAGE) gels.

Western blot (WB) analysis

The cells were lysed with a 2X SDS buffer consisting of 100 mM Tris–HCl (pH 6.8), 4% SDS, 20% glycerol, 200 mM β-mercaptoethanol, and 0.02% bromophenol blue. The protein extracts were then separated by SDS-PAGE and analyzed by western blotting, following previously established protocols [17].

Quantitative real-time reverse transcription polymerase chain reaction (qRT-PCR)

The qRT-PCR assay was performed according to previous report by minor modification [18]. After treatment, total RNA was isolated using a Tri-RNA reagent (Favorgen) and subsequently synthesized to complementary DNA by the reverse transcription 5X master mix (Eplisbio). The primer IL-1β, MCP-1, and heme oxygenase-1 (HO-1) were synthesized by BIONNER. Primer sequences are listed in Table 1. The relative gene expressions were calculated using the $2^{-\Delta\Delta ct}$ method, normalized by the housekeeping gene β-actin.

Luciferase reporter assay

Cells were co-transfected with pNF-κB-Luc or antioxidant response element (ARE)-Luc promoter and Renilla-Luc plasmid by the Solfect (Biosolyx) according to our previous report [5]. After transfection, cells were pretreated with 100 or 200 μM 6′-SL, 10 μM LY294002, or 10 μM SB 203580 for 1 h, followed by treatment with 1 μg/ml LPS for 12 h. Luciferase activity was evaluated by a dual-luciferase reporter assay system (E1960; Promega BioSystems Sunnyvale Inc.).

Immunofluorescence (IF) analysis

IF analysis was performed by the following previous report with minor modifications [19]. RAW 264.7 cells were seeded onto glass coverslips and treated with 1 μg/ml LPS, 100 or 200 μM 6′-SL, 10 μM LY294002, or 10 μM SB 203580 for 24 h in a 12-well plate. Cells were rinsed with PBS twice and fixed 4% paraformaldehyde for 10 min. Then, 0.2% Triton X-100 (JUNSEI) was added for 10 min for permeabilization at room temperature (RT). After blocking, RAW 264.7 cells were incubated with primary antibody against Nrf2 (1:200 dilution) overnight at 4°C and incubated with Alexa Fluor 488-conjugated secondary antibodies (1:250 dilution) for 1 h at RT. Finally, all cells were mounted with 4′,6-diamidino-2-phenylindole (DAPI) solution, and images were obtained using a K1-Fluo laser scanning confocal microscope (Nanoscope Systems). Fluorescence values were detected and merged using ImageJ.

Animals

Male ICR mice were obtained from SAMTAKO Inc. Mice were allowed to acclimate to the environment for one week before the start of the experiments and fed standard mice feed at 23°C ± 2°C, humidity (50% ± 5%), under a 12:12 dark:light cycle. All animal experiments were approved by with the Institutional Animal Care and Use Committee of Chungnam National University (202304A-CNU-063). Mice were randomly divided into 4 groups: group1, control; group 2, 10 mg/kg LPS; group 3, 100 mg/kg 6′-SL; group 4, 100 mg/kg 6′-SL + 10 mg/kg LPS. Mice were intraperitoneally (i.p.) administered 100 mg/kg 6′-SL for 2 h, except those in group 1 and 2. After 2 h, the mice were injected with 10 mg/kg LPS diluted in PBS *via* and i.p. injection for 6 h. Finally, the mice were sacrificed and aorta was collected.

En face IF staining

En face staining was employed to determine the expression of MCP-1 and MMP9 in mouse aortic endothelium according to a previously described method [12]. Mouse aortas were perfused with pre-chilled PBS followed by 4% paraformaldehyde. The harvested aortas were cleaned of fat and connective tissues, cut longitudinally, permeabilized with 0.2% Triton X-100 for 10 min, and blocked with 3% bovine serum albumin for 30 min at RT.

Table 1. List of primer sequences used for qRT-PCR

Name	Forward primer sequence (5′-3′)	Reverse primer sequence (3′-5′)
IL-1β	AACCTGCTGGTGTGTGACGTTC	CAGCACGAGGCTTTTTTGTTGT
MCP-1	CCACTCACCTGCTGCTACTCAT	TGGTGATCCTCTTGTAGCTCTCC
HO-1	ATGTGGCCCTGGAGGAGGAGA	CGCTGCATGGCTGGTGTGTAG
β-actin	CGTGCGTGACATCAAAGAGAA	TGGATGCCACAGGATTCCAT

qRT-PCR, quantitative real-time reverse transcription polymerase chain reaction; IL, interleukin; MCP-1, monocyte chemoattractant protein-1; HO-1, heme oxygenase-1.

Following the blocking process, cross-reactivity of primary antibodies with secondary antibodies was performed, in particular, aortas were incubated with primary antibodies against MCP-1 or MMP9 with VE-cadherin (1:250 dilution) overnight at 4°C and incubated with Alexa Fluor 488- or 546-conjugated secondary antibodies (1:250 dilution) for 1 h at RT. Finally, all aortas were mounted with DAPI solution, and images were obtained using a K1-Fluo laser scanning confocal microscope (Nanoscope Systems).

ROS determination on aortic endothelium

We performed *en face* staining to evaluate ROS expression in the mouse aortic endothelium according to our previous paper [8]. After sacrifice, mice were perfused with PBS to drain blood and harvest the thoracic aorta. The harvested aorta was cut open longitudinally, incubated with 40 mM DHE reagent in PBS for 60 min at 37°C, and washed with PBS. The aortas were then fixed with 4% paraformaldehyde for 10 min, washed with PBS, fat removed, and permeabilized with 0.2% Triton X-100 for 10 min. After washing with PBS, aortas were stained with DAPI (indicated nucleus). Images were acquired using a K1-Fluo laser scanning confocal microscope (Nanoscope Systems).

Statistical analysis

Statistical analyses were performed using GraphPad Prism 5 (version 5.02; GraphPad Software Inc.). One-way analysis of variance followed by Bonferroni multiple comparisons or two-tailed student's t-test was used for two group comparisons were performed. performed. All data are expressed as the mean ± standard error of the mean and all experiments were performed independently at least 3 times. $p<0.05$ was considered statistically significant.

RESULTS

Effect of 6'-SL on cell viability and Akt and p38 signaling pathway in RAW 264.7 cells

To investigate the effect of 6'-SL on cell survival in LPS-stimulated RAW 264.7 cells, cells were pretreated with 25, 50, 100, and 200 μM of 6'-SL for 1 h, followed by treatment with 1 μg/ml of LPS for 24 h after that cell viability was measured by MTT assay. As shown in Fig. 1A, both LPS stimulation and 6'-SL treatment demonstrated no cytotoxicity on RAW 264.7 cells. Next, we assessed the phosphorylation of Akt and p38 to evaluate inflammatory signaling pathways in the cells. LPS treatment led to increased phosphorylation levels of Akt and p38, while 6'-SL decreased the phosphorylation levels of both proteins in a dose-dependent manner compared to the LPS-treated group (Fig. 1B).

6'-SL inhibits LPS-induced inflammation by suppressing NF-κB translocation and transactivation in RAW 264.7 cells

The nuclear expression of NF-κB plays a pivotal role in the function of inflammatory mediators as a transcription factor [15]. To investigate whether 6'-SL inhibits the phosphorylation and translocation of NF-κB, cells were pretreated with 25, 50, 100, and 200 μM of 6'-SL for 1 h, followed by treatment with 1 μg/ml of LPS for 24 h. The activation of NF-κB p65 induced by LPS was inhibited by 50 μM of 6'-SL, with its activation steadily suppressed up to 200 μM of 6'-SL (Fig. 2A). The protein expression of PARP was used as a marker for nuclear extraction (Fig.

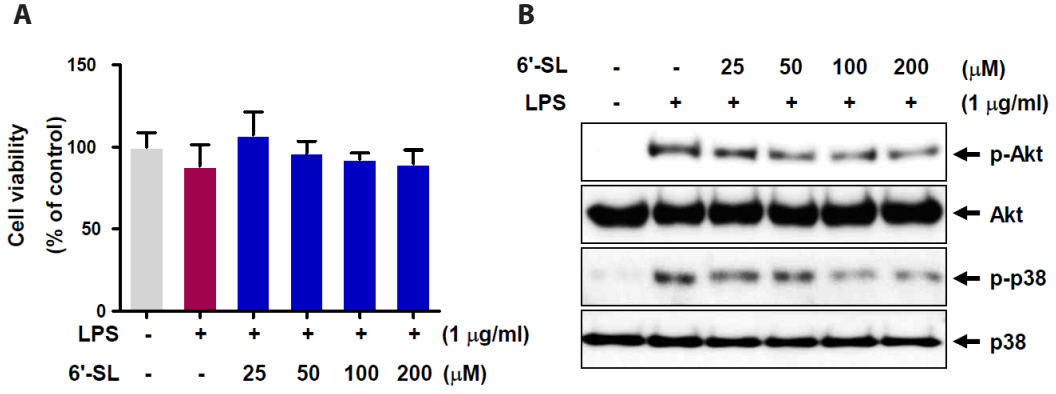

Fig. 1. Effect of 6′-SL on cell viability and Akt and p38 signaling pathway in RAW 264.7 cells. To determine the optimal concentration of 6′-SL for our experiments, we assessed the impact on inflammation signaling in RAW 264.7 cells *via* Western blotting. (A) RAW 264.7 cells were pre-exposed to 25, 50, 100, and 200 μM of 6′-SL for 1 h, followed by treatment with 1 μg/ml LPS for 24 h. Cell viability was assessed using the MTT assay. The results are presented as mean ± SEM, with n = 5 in each group. (B) RAW 264.7 cells were pre-treated with varying concentrations of 6′-SL for 1 h, followed by 1 μg/ml LPS treatment for 1 h. Total cell lysates were subjected to Western blot analysis using specific antibodies. 6′-SL, 6′-sialyllactose; Akt, protein kinase B; LPS, lipopolysaccharide; MTT, 3-(4,5-dimethylthiazole-2-yl)-2,5-diphenyltetrazolium bromide assay.

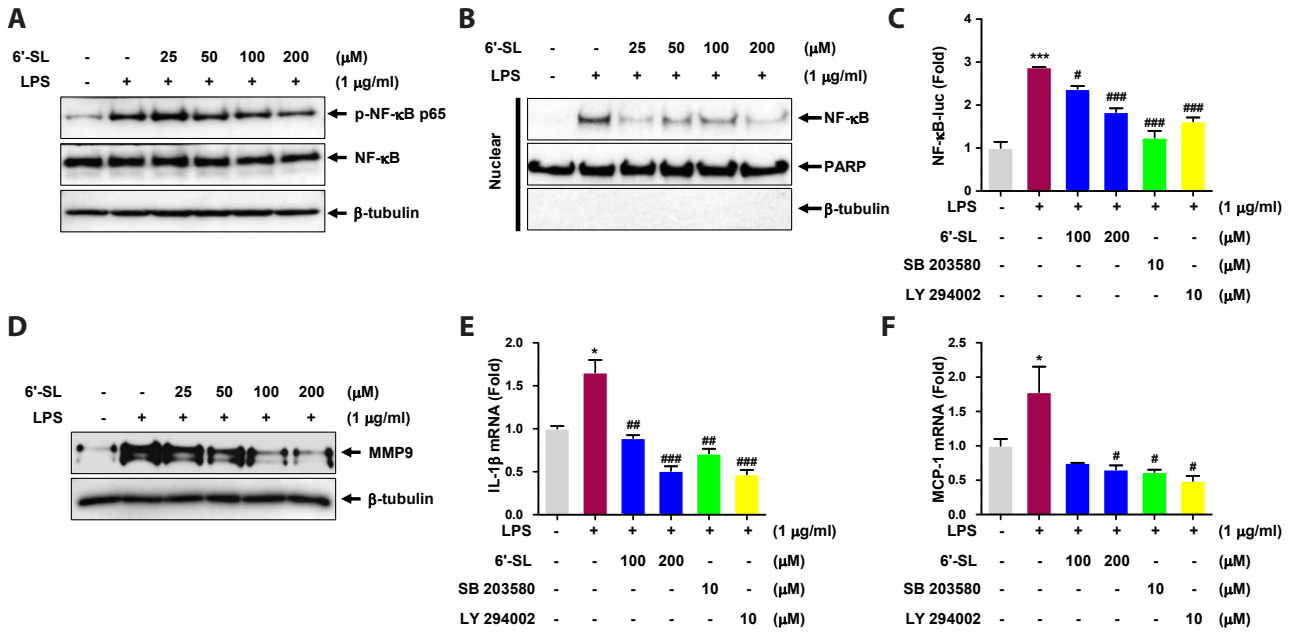

Fig. 2. 6′-SL inhibits LPS-induced inflammation by suppressing NF-κB translocation and transactivation in RAW 264.7 cells. The RAW 264.7 cells were exposed to varying concentrations of 6′-SL for 1 h, followed by treatment with 1 μg/ml LPS for 1 h. (A) Detect NF-κB phosphorylation of total cell, and then, protein expression was evaluated by Western blot. (B) Cells were subjected to nucleus fractionation to determine the amount of NF-κB in the nucleus. (C) RAW 264.7 cells were co-transfected with pNF-κB-Luc and Renilla-Luc for 24 h. After transfection, cells were pre-treated with 100 and 200 μM of 6′-SL, 10 μM of SB203580, and 10 μM of LY294002 for 1 h followed by treatment with 1 μg/ml LPS for 12 h. NF-κB-Luc promoter activity was measured using a dual-luciferase reporter assay. (D) RAW 264.7 cells were treated with the indicated concentrations of 6′-SL for 2 h, followed by treatment with 1 μg/ml LPS for 18 h. Protein expression of MMP9 was detected by Western blot. (E, F) The RAW 264.7 cells were treated with 100 and 200 μM of 6′-SL, 10 μM of SB203580, or 10 μM of LY294002 for 1 h, followed by treatment with 1 μg/ml LPS for 12 h. Total RNA samples were subjected to qRT-PCR using IL-1β (E) and MCP-1 (F) primers. Data are presented as the mean ± SEM (n = 4). 6′-SL, 6′-sialyllactose; LPS, lipopolysaccharide; NF-κB, nuclear factor kappa-light chain enhancer of activated B cells; MMP9, matrix metalloproteinase-9; qRT-PCR, quantitative real-time reverse transcription polymerase chain reaction; IL, interleukin; MCP-1, monocyte chemoattractant protein-1; PARP, poly ADP-ribose polymerase. *$p < 0.05$, ***$p < 0.001$ compared to the control group, $^{\#}p < 0.05$, $^{\#\#}p < 0.01$, $^{\#\#\#}p < 0.001$ compared to the LPS-treated group.

2B). Nuclear expression of NF-κB was completely abolished by pretreatment with 25 μM of 6'-SL (Fig. 2B), and this inhibitory effect was further enhanced by 200 μM of 6'-SL pretreatment (Fig. 2B). Consistent with the nuclear expression of NF-κB, the promoter activation of NF-κB was significantly increased by LPS, approximately 2-fold compared to the control (Fig. 2C). Interestingly, pretreatment with 200 μM of 6'-SL significantly suppressed LPS-induced NF-κB promoter activation to a similar extent as LY294002 (Fig. 2C). MMP9 is an enzyme crucial for macrophage migration, and its effects contribute to increased immune cell infiltration in the progression of atherosclerosis [2]. As shown in Fig. 2D, LPS stimulation markedly enhanced MMP9 expression, whereas its expression was consistently inhibited by 6'-SL. As downstream molecules of NF-κB and MMP9 in the inflammatory response, mRNA expression levels of IL-1β and MCP-1 were assessed *via* qRT-PCR. As anticipated, LPS treatment significantly upregulated the mRNA expression of IL-1β and MCP-1 by at least 1.5-fold compared to the control sample (Fig. 2E, F). Interestingly, pretreatment with 100 μM of 6'-SL completely suppressed LPS-mediated IL-1β and MCP-1 mRNA expression compared to the non-treated condition (Fig. 2E, F). Furthermore, this inhibition was comparable to the deactivation of Akt by LY294002 and p38 by SB203580 (Fig. 2E, F).

Antioxidative effects of 6'-SL in RAW 264.7 cells

Uncontrolled ROS production regulates multiple cellular mechanisms, including inflammation and cell apoptosis [7]. Therefore, to investigate the role of 6'-SL in LPS-induced ROS production, the treated cells were stained with DHE. LPS stimulation resulted in a 9-fold increase in the fluorescence intensity of DHE compared to the control (Fig. 3A). Treatment with 100 μM 6'-SL significantly reduced LPS-mediated ROS production by approximately 3-fold compared to the LPS-treated condition (Fig. 3B). Nrf2 serves as a key molecule in the antioxidant signaling pathway [14]. To verify this, we treated cells with LPS, SL, and kinase inhibitors, and examined Nrf2 nuclear translocation though IF analysis. As shown in Fig. 4A, Nrf2 clearly translocates into the nucleus in response to all stimuli except LPS. In contrast, LPS stimulation results in a slight increase in cytoplasmic expression of Nrf2 compared to the control (Fig. 4A, B). When Nrf2 expression was analysis by WB, LPS stimulation resulted in increased

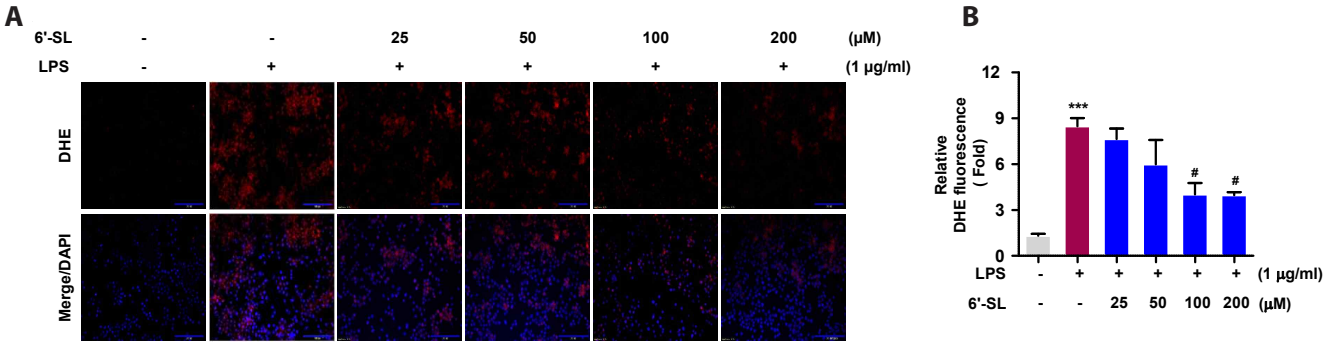

Fig. 3. Effect of 6-SL on LPS-induced ROS production. (A, B) The DHE assay showed a remarkable increase in ROS production in the cells. Raw 264.7 cells were pre-treated with 25, 50, 100, and 200 μM of 6′-SL for 1 h, followed by treatment with 1 μg/ml LPS for 24 h. The quantified graph indicates DHE fluorescence using ImageJ. Data are expressed as the mean ± SEM (n = 4). The scale bar represents 100 μm. 6′-SL, 6′-sialyllactose; LPS, lipopolysaccharide; ROS, reactive oxygen species; DHE, dihydroethidium; DAPI, 4′,6-diamidino-2-phenylindole. ***p < 0.001 compared to the control group, #p < 0.05 compared to the LPS-treated group.

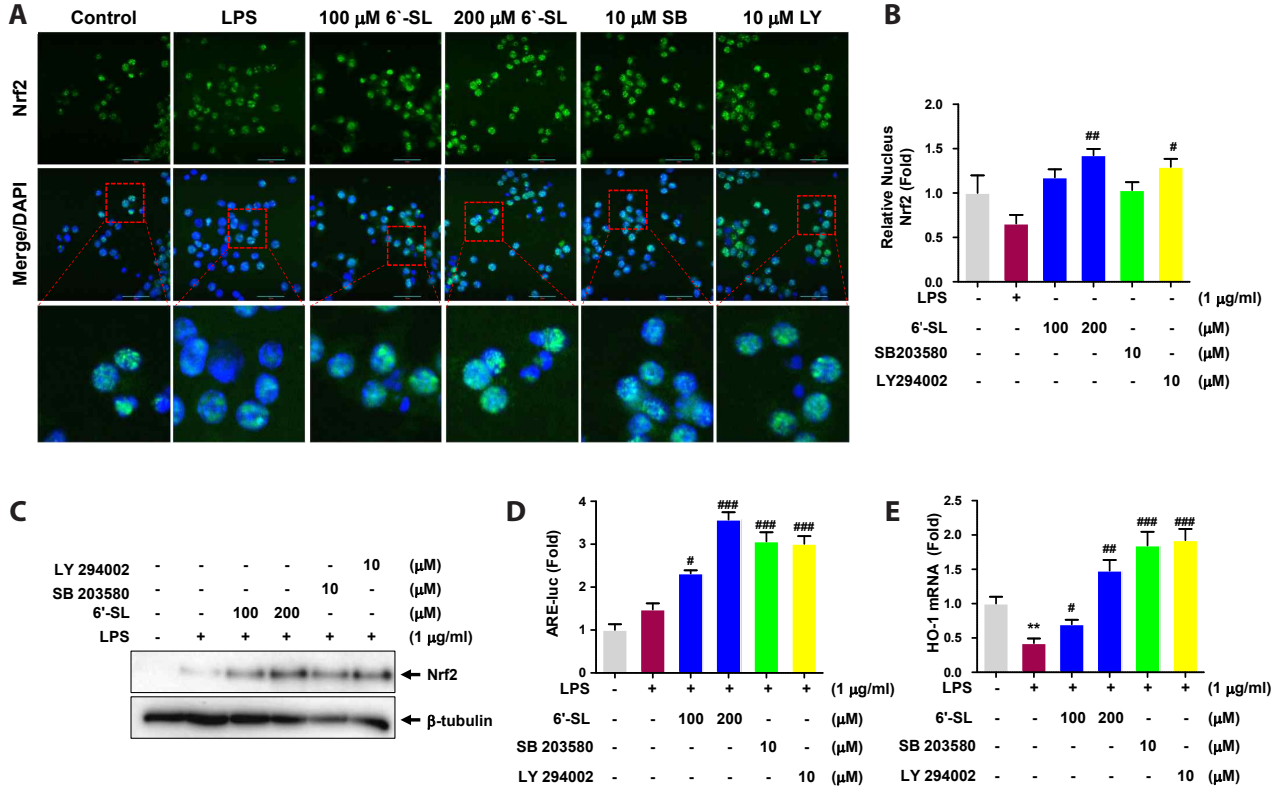

Fig. 4. Antioxidative effects of 6′-SL in RAW 264.7 cells. (A) RAW 264.7 cells were treated with 1 μg/ml LPS, 100 and 200 μM of 6′-SL, 10 μM of SB203580, or 10 μM of LY294002 for 24 h. Nrf2 translocation was analyzed by immunostaining with Nrf2 antibody. (B) Quantitively bar graph indicates relative fold change in nucleus Nrf2 expression. For quantification, cells within the sample images were enumerated based on DAPI-positive nuclei. The number of nucleus Nrf2-positive cells was then divided by the total cell count in each image. (C) RAW 264.7 cells were treated with 100 and 200 μM of 6′-SL, 10 μM of SB203580, or 10 μM of LY294002 for 1 h, followed by treatment with 1 μg/ml LPS for 24 h. Protein expression levels of Nrf2 and β-tubulin were detected by Western blot. (D) RAW 264.7 cells were co-transfected with ARE-Luc and Renilla-Luc for 24 h. After transfection, cells were pretreated with 100 and 200 μM of 6′-SL, 10 μM of SB203580, and 10 μM of LY294002 for 1 h, followed by treatment with 1 μg/ml LPS for 12 h. ARE-Luc promoter activity was measured using dual-luciferase reporter assay. (E) RAW 264.7 cells were treated with 100 and 200 μM of 6′-SL, 10 μM of SB203580, or 10 μM of LY294002 for 1 h, followed by treatment with 1 μg/ml LPS for 12 h. Total RNA samples were subjected to qRT-PCR using HO-1 primer. Data are expressed as the mean ± SEM (n = 3). 6′-SL, 6′-sialyllactose; LPS, lipopolysaccharide; Nrf2, nuclear factor erythoid 2-related factor 2; DAPI, 4′,6-diamidino-2-phenylindole; ARE, antioxidant response element; qRT-PCR, quantitative real-time reverse transcription polymerase chain reaction; HO-1, heme oxygenase-1. **p < 0.01 compared to the control group, #p < 0.05, ##p < 0.01, ###p < 0.001 compared to the LPS-treated group.

protein expression of Nrf2 (Fig. 4C). However, pretreatment with 100 and 200 μM of 6'-SL dose-dependently elevated Nrf2 expression levels (Fig. 4C). In the antioxidant signaling pathway, Nrf2 enhances the expression of antioxidant-related genes by binding to the ARE in the promoter region [13]. To investigate how 6'-SL activates the antioxidant signaling pathway, Nrf2 transcriptional activity was evaluated by ARE-luc reporter assay (Fig. 4D) and transcriptional target gene, HO-1 mRNA expression (Fig. 4E). As depicted in Fig. 4D, LPS treatment led to a slight increase in ARE promoter activity, while treatment with 100 μM of 6'-SL significantly enhanced ARE promoter activation. Consistent with the expression of Nrf2, 200 μM of 6'-SL further accelerated the antioxidant signaling pathway by inducing ARE promoter activity (Fig. 4D). In addition, the mRNA expression of HO-1, an antioxidant enzyme produced though Nrf2 transcription, was significantly increased at 200 μM of 6'-SL compared to the LPS-treated group (Fig. 4E).

6'-SL suppresses ROS production in mouse endothelium

To examine the effect of 6'-SL on macrophage-derived ROS production in LPS-activated mouse endothelium, isolated mouse aortas were stained with 40 mM DHE for 1 h, and the fluorescence intensity was measured by confocal microscopy (Fig. 5A). As shown in Fig. 5B, C, administration of LPS for 6 h significantly increased the number of DHE-stained ECs in the mouse endothelium. Consistent to *in vitro* data, 6'-SL significantly suppressed LPS-induced ROS production, similar to non-injected samples.

6'-SL suppresses ROS production in mouse endothelium 6'-SL inhibits LPS-induced MMP9 and MCP-1 expression in mouse endothelium

To further investigate the role of 6'-SL in LPS-induced macrophage inflammation, mouse aortas were isolated from wild-type ICR mice after i.p. injection with 10 mg/kg LPS for 6 h, and then the expression of MMP9 and MCP-1 was analyzed using *en face* IF assay. As depicted in Fig. 6A, LPS stimulation significantly increased the expression of MMP9 in EC cytoplasm in the s-flow area. Additionally, injection of 6'-SL significantly suppressed LPS-induced MMP9 expression (Fig. 6A). Consistent with the s-flow data, 6'-SL injection suppressed the LPS-accumulated expression of MMP9 in the d-flow area (Fig. 6B, C). To validate the anti-inflammatory effects of 6'-SL on mouse endothelium, MCP-1 expressions were assessed in both the s-flow and d-flow areas (Fig.

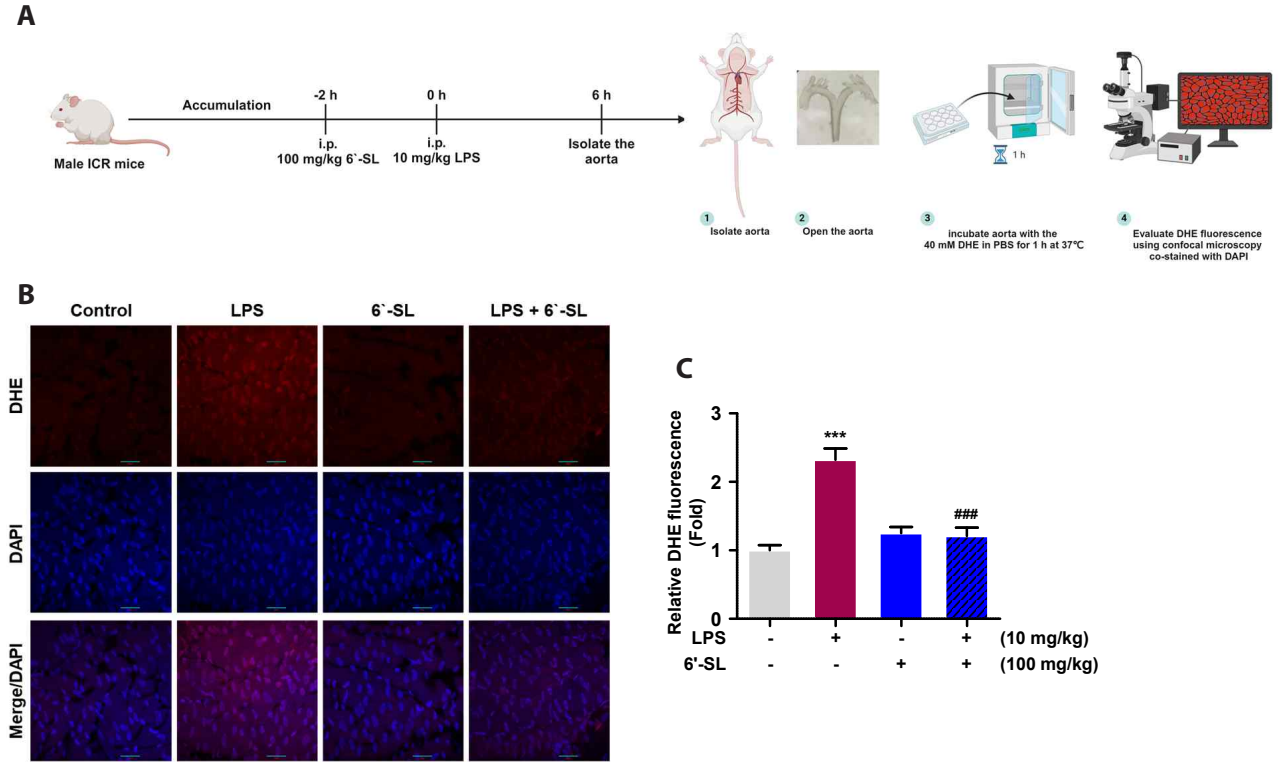

Fig. 5. 6′-SL suppresses ROS production in mouse endothelium. (A) Scheme of animal experiments and DHE staining on mouse endothelium. (B) The aorta was stained with DHE and nuclei were stained with DAPI. The scale bar indicates 30 μm. (C) The graph indicates DHE fluorescence using ImageJ. Data are expressed as the mean ± SEM (n = 3). 6′-SL, 6′-sialyllactose; ROS, reactive oxygen species; DHE, dihydroethidium; DAPI, 4′,6-diamidino-2-phenylindole; LPS, lipopolysaccharide; i.p., intraperitoneally. ***$p < 0.001$ compared with the control group, $^{###}p < 0.001$ compared with the LPS-treated group.

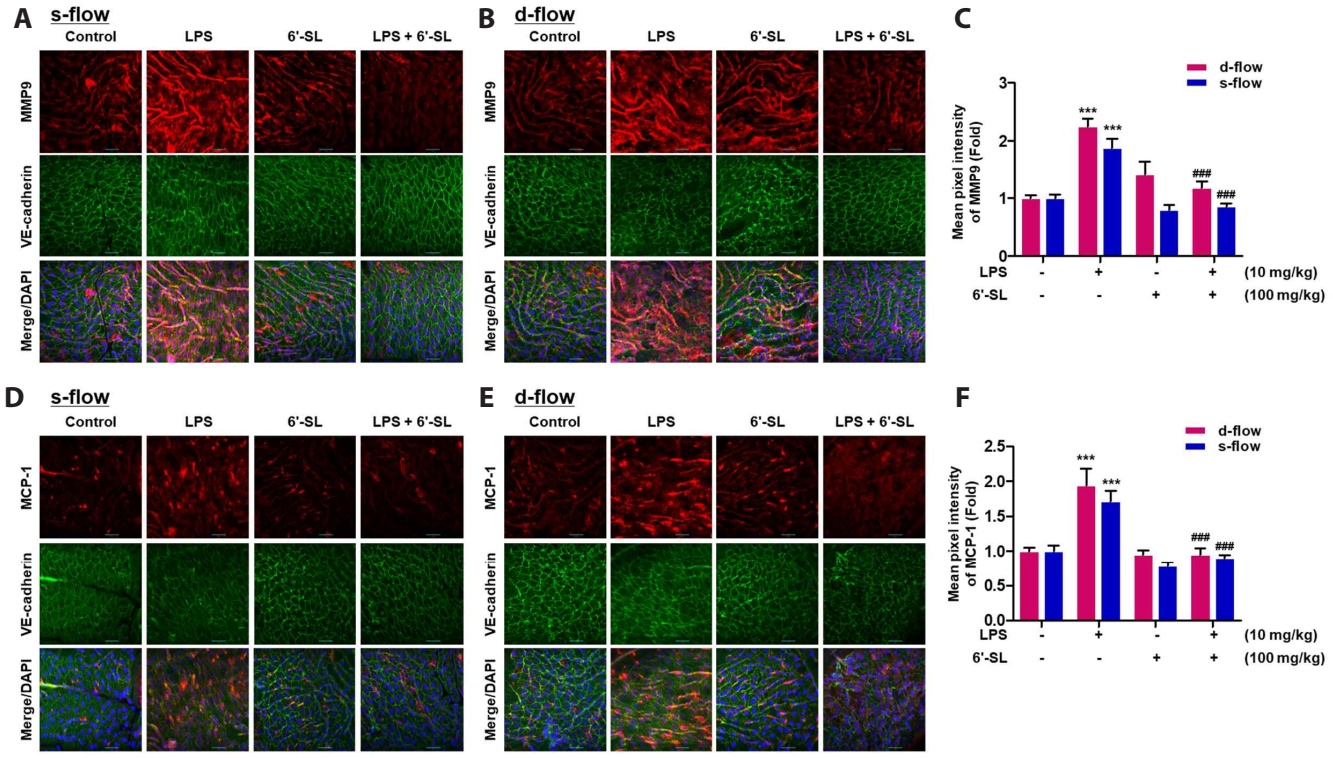

Fig. 6. 6′-SL inhibits LPS-induced MMP9 and MCP-1 expression in mouse endothelium. The mice were pretreated with 100 mg/kg of 6′-SL for 2 h prior to 10 mg/kg LPS for 6 h. Representative images of *en face* immunofluorescence staining of (A, B) MMP9 and (D, E) MCP-1 levels in the aorta endothelium of ICR mice. The endothelial junction was visualized though VE-cadherin staining, and nuclei were stained with DAPI. The scale bar indicates 30 μm. (C, F) The graph shows MMP9 and MCP-1 staining intensities in the mice aorta. Data are expressed as the mean ± SEM (n = 3). 6′-SL, 6′-sialyllactose; LPS, lipopolysaccharide; MMP9, matrix metalloproteinase-9; MCP-1, monocyte chemoattractant protein-1; VE-cadherin, vascular endothelial-cadherin; DAPI, 4′,6-diamidino-2-phenylindole. ***$p < 0.001$ compared with the control group, $^{###}p < 0.001$ compared with the LPS-treated group.

6D–F). LPS treatment increased the number of MCP-1-stained ECs and their expression. Whereas, injection of 6'-SL further inhibited LPS-induced MCP-1 expression in the s-flow area (Fig. 6D–F). Similar to the expression in the s-flow area, 6'-SL suppressed the LPS-induced fluorescence intensity and number of MMP9 and MCP-1-stained ECs in the d-flow area (Fig. 6D–F).

DISCUSSION

Regulating immune cell activation, particularly monocyte-to-macrophage differentiation, plays a pivotal role in inflammation. This is crucial because differentiated macrophages can infiltrate various organs, including the liver, kidney, or vessels, and subsequently release pro-inflammatory cytokines and chemokines [1,11,20]. Mechanistically, during macrophage migration to other cells, the expression of MMPs leads to destabilization of membrane junction protein expression [21]. In atherosclerosis models, overexpression of MMP9 in macrophages enhances acute plaque disruption, thereby increasing macrophage proteolytic activity and promoting plaque instability [21,22].

LPS is known to activate macrophage polarization to M1 or M2 and induce the release of pro-inflammatory cytokines such as tumor necrosis factor-α and IL-1β, as well as ROS or nitric oxide production [23,24]. Previous studies from our group have demonstrated that LPS stimulation leads to mRNA expression of pro-inflammatory cytokines, including IL-1β and MCP-1, though the activation of MAPK, signal transducer and activator of transcription, and NF-κB signaling pathways [4,8,11,15]. When LPS induces an inflammatory response, various signaling pathways are activated, leading to its mediated inflammatory response by enhancing its transcriptional activity [25].

Our data demonstrated that treatment with LPS significantly activates Akt and p38 signaling pathways, whereas, pretreatment with 6'-SL suppresses the phosphorylation of Akt and p38 induced by LPS in a dose-dependent manner, suggesting that 6'-SL has inhibitory effects on these pro-inflammatory pathways (Figs. 1B and 7). As downstream events, we further found that 6'-SL in modulating the NF-κB signaling pathway, a key activator of inflammatory mediators. 6'-SL abolishes the LPS-mediated nuclear expression and promoter activity of NF-κB at 100 μM (Fig. 2A–C).

Moreover, 6'-SL demonstrates dose-dependent inhibition of LPS-induced protein expression of MMP9, a crucial enzyme implicated in inflammatory processes (Fig. 2D). Consistent with

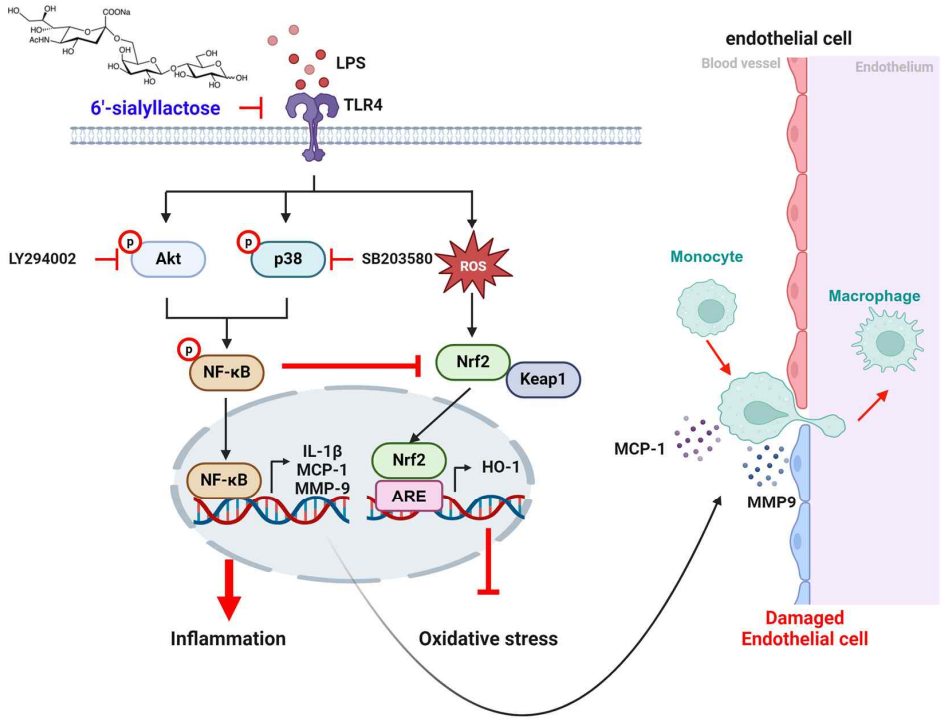

Fig. 7. Schematic illustration. The protective effect of 6′-sialyllactose in LPS-induced macrophage inflammation *via* regulating Nrf2-mediated oxidative stress and inflammatory signaling pathways. LPS, lipopolysaccharide; TLR4, Toll-like receptor 4; Akt, protein kinase B; ROS, reactive oxygen species; NF-κB, nuclear factor kappa-light chain enhancer of activated B cells; IL, interleukin; MCP-1, monocyte chemoattractant protein-1; MMP9, matrix metalloproteinase-9; Nrf2, nuclear factor erythoid 2-related factor 2; Keap1, kelch-like ECH-associated protein 1; ARE, antioxidant response element; HO-1, heme oxygenase-1.

this, pretreatment with 100 μM of 6'-SL significantly suppresses the mRNA expression of IL-1β and MCP-1, downstream molecules of NF-κB and MMP9, to a similar extent as inhibitors of Akt and p38 (Fig. 2E, F). In line with the *in vitro* findings, administration of LPS to mice results in a significant increase in the fluorescence intensity of MMP9 and MCP-1 in both d-flow and s-flow areas of isolated aortas (Fig. 6). However, injection of 6'-SL effectively suppresses the LPS-induced expression of MMP9 and MCP-1 in these areas (Fig. 6).

The balance between oxidant and antioxidant levels is crucial for macrophage polarization [26]. M1-type activation leads to the production of ROS and pro-inflammatory cytokines, which in turn increase the numbers and activation of macrophages [27]. Under non-stress conditions, ROS levels are kept at very low levels and tightly regulated within cells. When ROS levels are increasing by the stimuli, oxidative stress is prevented by the nuclear translocation of Nrf2, an antioxidant [13]. This occurs when Nrf2 dissociates from kelch-like ECH-associated protein 1 (KEAP1), reducing ROS production and repairing ROS-induced damage [13]. However, sustained excessive ROS levels lead to an increase in Nrf2 and KEAP1 in the cytosol but a decrease in Nrf2 nuclear translocation [28]. To verify this, we treated cells with LPS, SL, and kinase inhibitors, and examined Nrf2 nuclear translocation though IF analysis. As shown in Fig. 4A, Nrf2 clearly translocate into the nucleus in response to all stimuli except LPS. In contrast, LPS stimulation results in a slight increase in cytoplasmic expression of Nrf2 compared to the control (Fig. 4A, B). This suggests that the increase in Nrf2 protein expression induced by LPS, observed in the Western blotting data (Fig. 5C), is due to its expression in the cytoplasm rather than its activation in the nucleus. In the nucleus, Nrf2 binds to ARE in the promoter regions of various genes involved in antioxidant defense, detoxification, and cellular protection [13]. This binding induces the expression of these genes, thereby enhancing the cell's capacity to neutralize ROS and mitigate oxidative damage [13]. Therefore, Nrf2 transcriptional activity was evaluated by ARE-luc reporter assay (Fig. 4D) and transcriptional target gene, HO-1 mRNA expression (Fig. 4E). Our data showed that LPS treatment led to a slight increase in ARE promoter activity, while treatment with 100 μM of 6'-SL significantly enhanced ARE promoter activation. Consistent with the expression of Nrf2, 200 μM of 6'-SL further accelerated the antioxidant signaling pathway by inducing ARE promoter activity (Fig. 4D). In addition, the mRNA expression of HO-1, an antioxidant enzyme produced though Nrf2 transcription, was significantly increased at 200 μM of 6'-SL compared to the LPS-treated group (Fig. 4E). Therefore, it suggests that 6'-SL would reduce excessive ROS though antioxidant defense by Nrf2 transactivation and subsequent expression of HO-1.

p38 is a central regulator of the inflammatory response to both exogenous and endogenous injury [29] and contributes to mac-

rophage polarisation and migration though Akt phosphorylation [11]. It has been suggested that there is significant cross-talk between NF-κB and Nrf2 pathways [30,31]. For example, oxidative stress can activate NF-κB, which in turn can lead to an inflammatory response. On the other hand, Nrf2 activation can help to reduce oxidative stress and modulate inflammation, providing a balancing act between these two pathways. Our data indicates that activations of p38 and Akt are involved in NF-κB transactivation and regulates transcriptional targets, such as MMP9, IL-1β and MCP-1 (Fig. 2C–F). Consequently, during the inflammatory response, NF-κB is activated *via* Akt and p38, which acts to inhibit the activation of Nrf2.

Consistent to *in vitro* data, administration of 10 mg/kg LPS significantly increased the number of DHE-stained EC and the fluorescence intensity of DHE (Fig. 5C). Furthermore, 100 mg/kg 6'-SL significantly inhibited LPS-induced ROS production to a level comparable to the control condition (Fig. 5C). Together, 6'-SL demonstrates potent anti-inflammatory and antioxidant properties by inhibiting key signaling pathways involved in LPS-induced inflammation and oxidative stress.

Toll-like receptor (TLR)4 is the main receptor for LPS, and upon binding of LPS to TLR4, various cellular mechanisms are activated, leading to an increase in the expression of inflammatory mediator genes [11]. Previously, our group demonstrated that LPS treatment significantly increased the mRNA expression and production of pro-inflammatory cytokines by binding to TLR2 or TLR4 in macrophages or ECs [11] and [12]. Furthermore, pretreatment with 6-SL significantly suppressed LPS-induced TLR4 mRNA expression in ECs [14]. Therefore, it is possible that 6-SL blocks the binding of LPS to TLR4 and its inflammatory signaling pathway. In the future study, we will investigate how 6`-SL suppresses the LPS-mediated inflammatory signaling pathway using an LPS/TLR binding assay. By pursuing this future research plan, we can further elucidate the therapeutic potential of 6-SL as an anti-inflammatory agent and potentially develop novel treatment strategies for inflammatory diseases mediated by TLR4 activation.

FUNDING

This work was supported by National Research Foundation of Korea (KNRF-2022R1A2C4001776123148209264 0102).

ACKNOWLEDGEMENTS

None.

CONFLICTS OF INTEREST

Lila Kim is an employee of GeneChem Inc. The other authors have no conflict of interest.

REFERENCES

1. Eshghjoo S, Kim DM, Jayaraman A, Sun Y, Alaniz RC. Macrophage polarization in atherosclerosis. *Genes (Basel)*. 2022;13:756.
2. Hansson GK, Hermansson A. The immune system in atherosclerosis. *Nat Immunol*. 2011;12:204-212.
3. Jin Y, Heo KS. Experimental model and novel therapeutic targets for non-alcoholic fatty liver disease development. *Korean J Physiol Pharmacol*. 2023;27:299-310.
4. Jin Y, Jeon H, Le Lam Nguyen T, Kim L, Heo KS. Human milk oligosaccharides 3'-sialyllactose and 6'-sialyllactose attenuate LPS-induced lung injury by inhibiting STAT1 and NF-κB signaling pathways. *Arch Pharm Res*. 2023;46:897-906.
5. Jin Y, Tangchang W, Kwon OS, Lee JY, Heo KS, Son HY. Ginsenoside Rh1 ameliorates the asthma and allergic inflammation via inhibiting Akt, MAPK, and NF-κB signaling pathways in vitro and in vivo. *Life Sci*. 2023;321:121607.
6. Zhang JM, An J. Cytokines, inflammation, and pain. *Int Anesthesiol Clin*. 2007;45:27-37.
7. Huynh DT, Heo KS. Therapeutic effects of ginsenosides on vascular smooth muscle cell phenotypic switching in vascular diseases. *Cardiometab Syndr J*. 2022;2:96-107.
8. Nguyen DV, Jin Y, Nguyen TLL, Kim L, Heo KS. 3'-Sialyllactose protects against LPS-induced endothelial dysfunction by inhibiting superoxide-mediated ERK1/2/STAT1 activation and HMGB1/RAGE axis. *Life Sci*. 2024;338:122410.
9. Nguyen TLL, Jin Y, Kim L, Heo KS. Inhibitory effects of 6'-sialyllactose on angiotensin II-induced proliferation, migration, and osteogenic switching in vascular smooth muscle cells. *Arch Pharm Res*. 2022;45:658-670.
10. Chen Y, Waqar AB, Nishijima K, Ning B, Kitajima S, Matsuhisa F, Chen L, Liu E, Koike T, Yu Y, Zhang J, Chen YE, Sun H, Liang J, Fan J. Macrophage-derived MMP-9 enhances the progression of atherosclerotic lesions and vascular calcification in transgenic rabbits. *J Cell Mol Med*. 2020;24:4261-4274.
11. Huynh DTN, Baek N, Sim S, Myung CS, Heo KS. Minor ginsenoside Rg2 and Rh1 attenuates LPS-induced acute liver and kidney damages via downregulating activation of TLR4-STAT1 and inflammatory cytokine production in macrophages. *Int J Mol Sci*. 2020;21:6656.
12. Jin Y, Nguyen TLL, Myung CS, Heo KS. Ginsenoside Rh1 protects human endothelial cells against lipopolysaccharide-induced inflammatory injury through inhibiting TLR2/4-mediated STAT3, NF-κB, and ER stress signaling pathways. *Life Sci*. 2022;309:120973.
13. Jeon H, Jin Y, Myung CS, Heo KS. Ginsenoside-Rg2 exerts anticancer effects through ROS-mediated AMPK activation associated mitochondrial damage and oxidation in MCF-7 cells. *Arch Pharm Res*. 2021;44:702-712.
14. Nguyen TLL, Nguyen DV, Heo KS. Potential biological functions and future perspectives of sialylated milk oligosaccharides. *Arch Pharm Res*. 2024;47:325-340.

15. Van Nguyen D, Nguyen TLL, Jin Y, Kim L, Myung CS, Heo KS. 6'-Sialylactose abolished lipopolysaccharide-induced inflammation and hyper-permeability in endothelial cells. *Arch Pharm Res*. 2022;45:836-848.
16. Chang JW, Kim S, Lee EY, Leem CH, Kim SH, Park CS. Cell-cell contacts via N-cadherin induce a regulatory renin secretory phenotype in As4.1 cells. *Korean J Physiol Pharmacol*. 2022;26:479-499.
17. Huynh DTN, Heo KS. Rh1 abolishes MCF-7 cell growth via down-regulation of ROS-induced PKCδ/p38/ERK1/2 signaling pathway. *Drug Targets and Therapeutics*. 2022;1:19-26.
18. Jang EJ, Kim H, Baek SE, Jeon EY, Kim JW, Kim JY, Kim CD. HMGB1 increases RAGE expression in vascular smooth muscle cells *via* ERK and p-38 MAPK-dependent pathways. *Korean J Physiol Pharmacol*. 2022;26:389-396.
19. Meng RY, Li CS, Hu D, Kwon SG, Jin H, Chai OH, Lee JS, Kim SM. Inhibition of the interaction between Hippo/YAP and Akt signaling with ursolic acid and 3'3-diindolylmethane suppresses esophageal cancer tumorigenesis. *Korean J Physiol Pharmacol*. 2023;27:493-511.
20. Nguyen TLL, Huynh DTN, Jin Y, Jeon H, Heo KS. Protective effects of ginsenoside-Rg2 and -Rh1 on liver function through inhibiting TAK1 and STAT3-mediated inflammatory activity and Nrf2/ARE-mediated antioxidant signaling pathway. *Arch Pharm Res*. 2021;44:241-252.
21. Gough PJ, Gomez IG, Wille PT, Raines EW. Macrophage expression of active MMP-9 induces acute plaque disruption in apoE-deficient mice. *J Clin Invest*. 2006;116:59-69.
22. Li T, Li X, Feng Y, Dong G, Wang Y, Yang J. The role of matrix metalloproteinase-9 in atherosclerotic plaque instability. *Mediators Inflamm*. 2020;2020:3872367.
23. Bobryshev YV, Ivanova EA, Chistiakov DA, Nikiforov NG, Orekhov AN. Macrophages and their role in atherosclerosis: pathophysiology and transcriptome analysis. *Biomed Res Int*. 2016;2016:9582430.
24. Wang Y, Liu H, Zhao J. Macrophage polarization induced by probiotic bacteria: a concise review. *Probiotics Antimicrob Proteins*. 2020;12:798-808.
25. Li J, Qin Y, Chen Y, Zhao P, Liu X, Dong H, Zheng W, Feng S, Mao X, Li C. Mechanisms of the lipopolysaccharide-induced inflammatory response in alveolar epithelial cell/macrophage co-culture. *Exp Ther Med*. 2020;20:76.
26. Tsai CF, Chen GW, Chen YC, Shen CK, Lu DY, Yang LY, Chen JH, Yeh WL. Regulatory effects of quercetin on M1/M2 macrophage polarization and oxidative/antioxidative balance. *Nutrients*. 2021;14:67.
27. Tan HY, Wang N, Li S, Hong M, Wang X, Feng Y. The reactive oxygen species in macrophage polarization: reflecting its dual role in progression and treatment of human diseases. *Oxid Med Cell Longev*. 2016;2016:2795090.
28. Saha S, Buttari B, Panieri E, Profumo E, Saso L. An overview of Nrf2 signaling pathway and its role in inflammation. *Molecules*. 2020;25:5474.
29. Perdiguero E, Sousa-Victor P, Ruiz-Bonilla V, Jardí M, Caelles C, Serrano AL, Muñoz-Cánoves P. p38/MKP-1-regulated AKT coordinates macrophage transitions and resolution of inflammation during tissue repair. *J Cell Biol*. 2011;195:307-322.
30. Ci X, Zhou J, Lv H, Yu Q, Peng L, Hua S. Betulin exhibits anti-inflammatory activity in LPS-stimulated macrophages and endotoxin-shocked mice through an AMPK/AKT/Nrf2-dependent mechanism. *Cell Death Dis*. 2017;8:e2798.
31. Yang H, Lv H, Li H, Ci X, Peng L. Oridonin protects LPS-induced acute lung injury by modulating Nrf2-mediated oxidative stress and Nrf2-independent NLRP3 and NF-κB pathways. *Cell Commun Signal*. 2019;17:62.